Inorganic Chemistry

Article pubs.acs.org/IC

Synthesis and Characterization of Cu(II) and Mixed-Valence Cu(I)Cu(II) Clusters Supported by Pyridylamide Ligands

Joseph D. Schneider, Brett A. Smith, Grant A. Williams, Douglas R. Powell, Felio Perez, Gerard T. Rowe,* and Lei Yang*



Cite This: Inorg. Chem. 2020, 59, 5433-5446



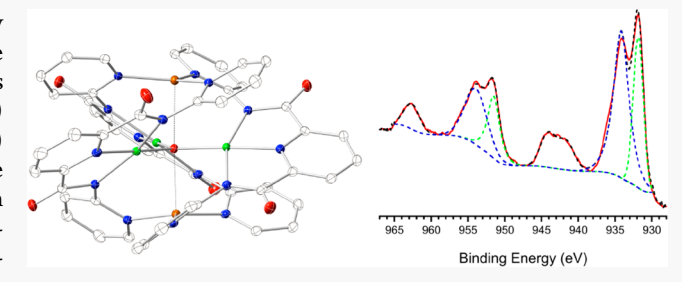
ACCESS

III Metrics & More

Article Recommendations

s Supporting Information

ABSTRACT: A group of copper complexes supported by polydentate pyridylamide ligands H₂bpda and H₂ppda were synthesized and characterized. The two Cu(II) dimers $[Cu^{II}_{2}(Hbpda)_{2}(ClO_{4})_{2}]$ (1) and $[Cu^{II}_{2}(ppda)_{2}(DMF)_{2}]$ (2) were constructed by using neutral ligands to react with Cu(II) salts. Although the dimers showed similar structural features, the second-sphere interactions affect the structures differently. With the application of Et₃N, the tetranuclear cluster (HNEt₃)- $[Cu^{II}_{4}(bpda)_{2}(\mu_{3}-OH)_{2}(ClO_{4})(DMF)_{3}](ClO_{4})_{2}$ (3) and hexanuclear cluster (HNEt₃)₂[Cu^{II}₆(ppda)₆(H₂O)₂(CH₃OH)₂](ClO₄)₂



(4) were prepared under similar reaction conditions. The symmetrical and unsymmetrical arrangement of the ligand donors in ligands H₂bpda and H₂ppda led to the dramatic conformation difference of the two Cu(II) complexes. As part of our effort to explore mixed-valence copper chemistry, the triple-decker pentanuclear cluster $\left[\text{Cu}^{\text{II}}_{3}\text{Cu}^{\text{I}}_{2}(\text{bpda})_{3}(\mu_{3}\text{-}0)\right]$ (5) was prepared. XPS examination demonstrated the localized mixed-valence properties of complex 5. Magnetic studies of the clusters with EPR evidence showed either weak ferromagnetic or antiferromagnetic interactions among copper centers. Due to the trigonal-planar conformation of the trinuclear Cu(II) motif with the μ_3 -O center, complex 5 exhibits geometric spin frustration and engages in antisymmetric exchange interactions. DFT calculations were also performed to better interpret spectroscopic evidence and understand the electronic structures, especially the mixed-valence nature of complex 5.

INTRODUCTION

In biological systems, active sites with multiple copper centers play vital roles in processes involving electron transfer and catalytic functions. For instance, a binuclear Cu_A site in cytochrome c oxidase (CcO) receives and transfers electrons between soluble cytochrome c and cytochrome a. The catalytic site of multicopper oxidases (MCOs) is a trinuclear copper cluster that oxidizes organic substrates and metal ions.² In nitrous oxide reductase (N_2OR), a μ_4 -sulfido-bridged tetranuclear copper cluster is the binding and reduction site for the two-electron reduction of N2O to N2 in the last step of bacterial denitrification.³ For copper-dependent particulate methane monooxygenase (PMMO), the nuclearity of the copper binding site has been intensely studied in an effort to identify the catalytic nature of this metalloenzyme. In addition to the extensive spectroscopic and computational studies regarding these copper proteins, the assembly and construction of bioinspired small molecular models have also been the subject of vigorous research in order to better understand the functional mechanisms of the copper proteins and use the clusters as potential catalysts. 5-8 One of the major focuses of these research studies is the mixed-valence intermediate(s) involved in the these processes. For instance, recent reports on binuclear Cu^{II}Cu^{III} complexes postulated the presence of such

a mixed-valence species in the oxidative process of Cu/O₂ chemistry. 9-13 In the activation chemistry of small molecules such as hydrocarbons, 14 H₂O, 15 NO, 16 N₂O, 17-23 and CO2, 24,25 localized and delocalized mixed-valence copper complexes have also been identified as critical intermediate species during the oxidation/reduction process.

The research in our group focuses on the valence intermediates of copper clusters supported by flexible pyridylamide ligands and their potential catalytic function. Our previous study has demonstrated that the combination of pyridyl and amidate nitrogen donors showed excellent coordination capabilities toward Cu(II) centers.²⁶ In addition, an interesting noncovalent interaction involving amide groups in the second-sphere coordination environment also contributed to the stabilization of the clusters. 27,28 In our recent work on copper complexes with CuICuI, CuI.5CuI.5, Cu^{1.5}Cu^{1.5}Cu^I, and Cu^{II}Cu^{II} cores, we found that copper

Received: January 2, 2020 Published: April 2, 2020





centers with various oxidation states can be stabilized by the same dipyridylamide ligand H,pcp (Scheme 1).²⁹ On the basis

Scheme 1. Pyridylamide Ligands H_2 bpda and H_2 ppda Used in This Work

of these results, we reasoned that the polydentate coordination modes and conformational flexibility of the ligand are the major contributing factors to the formation of these clusters. With the objective of nuclearity control and more diverse valence intermediates, we recently focused on using the ligand H₂bpda with the idea of introducing more ligand donors that can be used to manipulate the structural conformation of the resulting copper complexes. In an attempt to better understand the effect of ligand donors on the coordination behavior, we also investigated the copper chemistry of the ligand H₂ppda with an unsymmetrical arrangement of nitrogen donors in order to compare its coordination behavior with that of the ligand H₂bpda. In this paper, we report the synthesis and characterization of multinuclear Cu(II) and mixed-valence copper complexes supported by both ligands. X-ray structures demonstrated that the nuclearity could be controlled by the reaction conditions. Spectroscopic characterization provided evidence about the electronic structures of the complexes, especially the localized mixed-valence nature of a pentanuclear cluster. In addition, magnetic studies coupled with EPR data and computation work were conducted to examine the interaction among the copper centers.

EXPERIMENTAL SECTION

General Considerations. All reagents were obtained from commercial sources and used as received unless otherwise noted. The ligands N_1N' -bis(2-pyridyl)pyridine-2,6-dicarboxamide (H_2 bpda) and N-(phenyl)-N'-(2-pyridyl)pyridine-2,6-dicarboxamide (H₂ppda) were synthesized according to the literature.³⁰ UV-vis spectra were recorded on a Cary 50 spectrometer. Solid-state electronic reflectance spectra were collected by using an external remote diffuse reflectance accessory (DRA) with a 1.5 m long fiber optical probe which can scan an area less than 1.5 mm in diameter. MgO was used as a blank, and the fine powders of the complexes were used as samples directly without dilution. X-band EPR spectra were recorded on a Freiberg Instruments MiniScope MS5000 instrument. Elemental analyses were carried out by Atlantic Microlabs, Norcross, GA. FT-IR spectra were collected on a Nicolet Magna 560 FT-IR spectrometer with an ATR attachment. ¹H and ¹³C NMR spectra of the ligand were measured on a Bruker AVANCE 300 MHz spectrometer at room temperature. Cyclic voltammograms were measured using an EG&G Princeton Applied Research Scanning Potentiostat with a Pt-disk working electrode, Pt-wire auxiliary electrode, and Ag/AgCl glass reference electrode. All measurements were performed in organic solutions containing 1.0 mM analyte and 0.1 M NBu₄·BF₄ at room temperature with N2 protection. Recrystallized ferrocene was used as the internal standard. Mass spectra were collected on a Micromass MALDI-TOF MS instrument. The complexes were dissolved in organic solvents, and 2 μ L of the solutions was placed on a stainless steel sample well and allowed to dry at room temperature. No matrix was used for measurement. SQUID data were collected by using a Quantum Design MPSM 3 instrument.

CAUTION! The perchlorate salt $Cu(ClO_4)_2$ ·6 H_2O is potentially explosive. Although we did not experience any problems while conducting the work, it should be handled with great caution.

For X-ray photon spectroscopic measurements, analysis of the samples was performed using a Thermo Scientific K-Alpha XPS system equipped with a monochromatic X-ray source at 1486.6 eV, corresponding to the Al K line. An X-ray power of 75 W at 12 kV was used for all experiments with a spot size of 400 μ m². The base pressure of the K-Alpha instrument was at 1.0×10^{-9} mbar. The instrument was calibrated to give a binding energy of 84.0 eV for Au $4f_{7/2}$ and 284.8 eV for the C 1s line of adventitious (aliphatic) carbon present on the nonsputtered samples. Photoelectrons were collected from a takeoff angle of 90° relative to the sample surface. Measurements were done in the Constant Analyzer Energy mode. The survey spectra were taken at a pass energy of 200 eV, while the high-resolution (HR) core level spectra were taken at a 40 eV pass energy with an energy step size of 0.1 eV and an average of 30 scans. The XPS data acquisition was performed using the Advantage v5.932 software provided with the instrument.

N-(Phenyl)-N'-(2-pyridyl)pyridine-2,6-dicarboxamide (H₂ppda). 2,6-Pyridinedicarbonyl dichloride (2.041 g, 10.00 mmol) was dissolved in pyridine, and a 2 mL pyridine solution of aniline (0.931 g, 1.00 mmol) was added to the mixture at 55 °C. The mixture was stirred for about 1 h, and a 2 mL pyridine solution of 2aminopyridine (0.941 g, 1.00 mmol) was added. After overnight stirring, 450 mL of distilled water was added to the mixture. The raw product was collected by filtration and rinsed with a saturated NaHCO₃ solution (150 mL \times 3) and distilled water (100 mL \times 3). Recrystallization of the product in CH3CN at low temperature afforded light brown crystals (1.15 g, 36.1%). ¹H NMR (DMSO- d_6): δ 11.01 (s, 2H, NH), 7.18–8.38 (m, 12H) ppm. $^{13}\mathrm{C}$ NMR (DMSO d_6): δ 13.03, 162.46, 162.20, 149.41, 148.65, 140.41, 138.87, 138.56, 129.33, 126.23, 125.57, 124.96, 122.23, 121.69 ppm. Anal. Calcd for C₁₈H₁₄N₄O₂: C, 67.91; H, 4.43; N, 17.60. Found: C, 67.63; H, 4.60; N, 17.42. FT-IR (cm⁻¹): 3268, 1672, 1652, 1590, 1531, 1496, 1447, 1437, 1334, 1241, 1158, 1144, 1079, 1030, 1000, 948, 905, 881, 837, 783, 754, 735, 719, 683, 650, 593, 582, 505, 423.

[Cu^{II}₂(Hbpda)₂(ClO₄)₂] (1). Cu(ClO₄)₂·6H₂O (0.029 g, 0.078 mmol) was added to a stirred solution of H₂bpda (0.025 g, 0.078 mmol) in 2 mL of CH₃OH. The green suspension was stirred for 2 h, and 20 mL of Et₂O was added to the mixture. The resulting green powder was collected and washed with Et₂O (5 mL × 3). The raw product was dissolved in 2 mL of CH₃CN and filtered. Vapor diffusion of Et₂O into the green solution at room temperature led to the formation of green crystals suitable for X-ray crystallographic characterization (0.031 g, 76% yield). Anal. Calcd for C₃₄H₂₄N₁₀O₁₂Cl₂Cu₂: C, 42.42; H, 2.51; N, 14.55. Found: C, 42.09; H, 2.70; N, 14.48. FT-IR (cm⁻¹): 1600, 1548, 1488, 1421, 1373, 1308, 1208, 1083, 1054, 1026, 1003, 962, 945, 904, 868, 838, 809, 783, 760, 688, 602, 544, 497, 464, 429. UV-vis (λ_{max} , nm (ε , M⁻¹ cm⁻¹)): CH₃CN, 668 (398); DMF, 657 (342).

[Cu^{II}₂(ppda)₂(DMF)₂] (2). Cu(OAc)₂ (0.011 g, 0.063 mmol) was added to a stirred solution of H₂ppda (0.020 g, 0.063 mmol) in 2 mL of DMF. The deep green mixture was stirred for 3 h, and 15 mL of Et₂O was added to the mixture. The resulting green powder was collected and washed with Et₂O (5 mL × 3). The raw product was extracted with 2 mL of DMF and filtered. Vapor diffusion of Et₂O into the green solution at room temperature led to the formation of dark blue crystals suitable for X-ray crystallographic characterization (0.012 g, 42% yield). Anal. Calcd for C₄₂H₃₈N₁₀O₆Cu₂: C, 55.68; H, 4.23; N, 15.46. Found: C, 55.40; H, 4.18; N, 15.86. FT-IR (cm⁻¹): 1660, 1626, 1609, 1574, 1545, 1527, 1468, 1430, 1386, 1348, 1315, 1294, 1253, 1157, 1096, 1071, 1018, 963, 925, 888, 842, 789, 763, 748, 687, 678, 658, 531, 483, 429. UV-vis (λ_{max} , nm (ε , M⁻¹ cm⁻¹)): DMF, 668 (280).

(HNEt₃)[Cu^{II}₄(bpda)₂(μ_3 -OH)₂(ClO₄)(DMF)₃](ClO₄)₂ (3). Cu-(ClO₄)₂·6H₂O (0.116 g, 0.31 mmol) was added to a stirred mixture of H₂bpda (0.050 g, 0.16 mmol) and Et₃N (0.048 g, 0.47 mmol) in 2 mL of methanol. The deep green suspension was stirred for 2 h, and 20 mL of Et₂O was added to the mixture. The resulting green powder

was collected and washed with Et₂O (5 mL × 3). The powder was dissolved in 4 mL of DMF and filtered. Layering Et₂O on top of the deep green solution at room temperature and slow diffusion led to the formation of dark green crystals suitable for X-ray crystallographic characterization (0.094 g, 74% yield). Anal. Calcd for C₄₉H₆₁N₁₄O₂₁Cl₃Cu₄: C, 38.15; H, 3.99; N, 12.71. Found: C, 38.29; H, 4.08; N, 13.07. FT-IR (cm¹): 2934, 2360, 1637, 1597, 1563, 1479, 1432, 1363, 1320, 1294, 1252, 1167, 1075, 925, 887, 838, 777, 758, 668, 621, 530. UV–vis ($\lambda_{\rm max}$) nm (ε , M⁻¹ cm⁻¹)): CH₃CN, 648 (344); DMF, 640 (231).

(HNEt₃)₂[Cu^{II}₆(ppda)₆(H₂O)₂(CH₃OH)₂](ClO₄)₂ (4). Cu(ClO₄)₂. 6H₂O (0.025g, 0.067 mmol) was added to a mixture of H₂ppda (0.020 g, 0.063 mmol) and Et₃N (0.013 g, 0.13 mmol) in 2 mL of methanol. The deep green solution was stirred for 1 h and was then filtered through a Celite plug. Vapor diffusion of Et₂O into the green filtrate at room temperature led to the formation of dark green crystals suitable for X-ray crystallographic characterization (0.0148 g, 49% yield). Anal. Calcd for C₁₂₂H₁₁₆N₂₆O₂₄Cl₂Cu₆: C, 52.66; H, 4.20; N, 13.09. Found: C, 52.89; H, 4.65; N, 13.51. FT-IR (cm⁻¹): 1597, 1540, 1473, 1439, 1392, 1316, 1069, 929, 870, 837, 792, 756, 696, 621, 506, 439. UV—vis (λ_{max} , nm (ε , M⁻¹ cm⁻¹)): CH₃OH, 639 (541); DMF, 630 (554).

 $[Cu^{II}_{3}Cu^{I}_{2}(bpda)_{3}(\mu_{3}-O)]$ (5). Under N₂, NaH (0.0056 g, 0.24) mmol) was added to 2 mL of a DMF solution of H₂bpda (0.025 g, 0.078 mmol) with H_2O (1.4 μ L, 0.078 mmol) in a Schlenk flask. After 1 h of stirring, Cu(OTf)₂ (0.028 g, 0.078 mmol) was added, followed by the addition of CuCl (0.0052 g, 0.052 mmol). The mixture was stirred for about 2 h, and 20 mL of degassed Et₂O was added. The supernatant was removed by using a pipet, and the resulting deep green solid was dried under vacuum. The raw product was transferred into a glovebox and washed with Et₂O (5 mL \times 3). The deep green powder was dissolved in 2 mL of DMF and filtered. Vapor diffusion of Et₂O into the dark green solution at room temperature led to the formation of deep green crystals suitable for X-ray crystallographic characterization (0.020 g, 52% yield). Anal. Calcd for C₅₁H₃₃N₁₅O₇Cu₅: C, 47.65; H, 2.59; N, 16.34. Found: C, 47.88; H, 2.41; N, 15.98. FT-IR (cm⁻¹): 1659, 1612, 1601, 1583, 1553, 1465, 1423, 1359, 1305, 1279, 1158, 1093, 1076, 1053, 1008, 963, 914, 873, 838, 786, 768, 749, 682, 659, 639, 588, 548, 533, 449, 418. UV-vis $(\lambda_{\text{max}} \text{ nm } (\varepsilon, \text{ M}^{-1} \text{ cm}^{-1}))$: CH₂Cl₂, 573 (420), 790 (shoulder, 230); DMF, 578 (502), 780 (shoulder, 261).

X-ray Crystallography. X-ray crystallographic data were collected on crystals with dimensions of $0.150 \times 0.130 \times 0.120$ mm for 1, $0.12 \times 0.19 \times 0.36$ mm for 2, $0.430 \times 0.380 \times 0.250$ mm for 3, and $0.200 \times 0.230 \times 0.320$ mm for 5. Data were collected at 100 K using a diffractometer with a Bruker APEX CCD area detector³¹ and graphite-monochromated Mo K α radiation ($\lambda = 0.71073$ Å). All four structures were solved by direct methods and refined by full-matrix least-squares methods on $F^{2,32,33}$ The crystal parameters, data collection and refinement of 1–3 and 5 are summarized in Table S1.

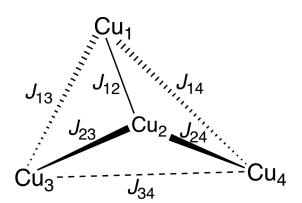
Hirshfeld Surface Analysis. In order to investigate the important intra- and intermolecular interactions occurring within and among the coordination units, the analysis of Hirshfeld surfaces was performed by using CrystalExplorer (version 3.0) software.³⁴ The calculation was based on the CIF files from the X-ray crystal structures of the metal complexes.

Magnetic Susceptibility and Magnetic Data Fitting. The magnetic susceptibilities of complexes 1, 3, and 5 were measured using a Quantum Design MPMS SQUID VSM Evercool magnetometer. The sample was loaded into a polypropylene VSM powder holder. The magnetic susceptibility (zero-field cooled) was measured with an applied field of 1000 Oe as a function of temperature between 2 and 300 K. The methods of Morrison et al. were used to correct for shape and radial offset effects. The program PHI 3.1.1 was used to fit magnetic data to an appropriate model Hamiltonian.

The magnetic susceptibilities of complexes 1, 3, and 5 were each fit to a phenomenological exchange Hamiltonian, as determined with PHI 3.1.1. For complex 1, an intermolecular exchange interaction term (zJ) was modeled through the mean-field approximation. For complex 3, the copper(II) ions were modeled as octahedral centers

using the *J*-coupling scheme shown in Scheme 2. Parameters for complexes 1 and 5 were determined through simultaneous fitting of

Scheme 2. *J*-Coupling Scheme Used to Model the Magnetic Susceptibility of Complex 3



$$Cu_1 = Cu_2$$
, $Cu_3 = Cu_4$
 $J_{12} = J_8$
 $J_{13} = J_{14} = J_{23} = J_{24} = J_m$
 $J_{34} = J_L$

their respective magnetic susceptibility and EPR data. Accurate fitting of the magnetic behavior of complex 5 was achieved by including an antisymmetric exchange term in the model Hamiltonian with the Cu(II) ions modeled as three equivalent Cu(II) centers with an octahedral geometry.

Computational Chemistry. All electronic structure calculations were carried out with Orca 4.1.0 for Linux.³⁷ VMD³⁸ was used for visualization of orbitals and density plots and rendered using the Tachyon library.³⁹ NBO 3.1 population analysis was carried out with Gaussian 09.⁴⁰ Starting with the structure obtained from X-ray crystallography analysis, the optimized geometry of complex 5 was calculated at the M06-L⁴¹/def2-SVP⁴² level of theory with the auxiliary basis set def2/J⁴³ used for the RI approximation. Grimme's dispersion correction (D3zero) was applied to the geometry optimization calculations.^{44,45} To correct for basis set superposition error, all calculations employed the geometrical counterpoise correction (gCP).⁴⁶ The identification of the compound's structural minimum was confirmed through the absence of imaginary vibrational modes in a numerical frequency calculation.

The XPS spectrum of complex **5** was interpreted by analysis of its Cu 2p orbitals in a single-point calculation carried out at the optimized geometry. This calculation was carried out at the M06-L/def2-TZVP level of theory with the exception of copper atoms, for which the polarized CoreProp basis set (CP(PPP)) was utilized. A higher accuracy integral grid (Lebedev 770 point grid) was also utilized for the copper atoms. To aid in comparison of the copper 2p orbital energies, the restricted-open wave function was calculated.

The gas-phase electronic spectrum of complex 5 was calculated using TD-DFT at the B3LYP/def2-SVP level of theory with the RIJCOSX⁴⁹ and Tamm—Dancoff approximations enabled. The first 200 excited states were included in the calculation to cover the experimental spectral range. Visualization of selected electronic excitations was achieved through the use of TD-DFT difference densities. For the states of interest, the electronic transitions were too complex for the individual contributions to the excitation to be interpreted, even when natural transition orbitals were employed.

■ RESULTS AND DISCUSSION

X-ray Crystal Structures. When the neutral ligand H_2 bpda reacted with $Cu(ClO_4)_2$ · $6H_2O$ in CH_3OH , green crystals were afforded by recrystallization of the raw product through Et_2O diffusion. X-ray crystallographic analysis of complex 1 showed a dimeric structure with two Cu(II) centers, two monoanionic $Hbpda^-$ ligands, and two weakly coordinated ClO_4^- anions. (Figure 1 left). For Cu(II) centers, the N_4O coordination environment forms a distorted-square-pyramidal geometry with a τ_5 value of 0.24. The axial position is occupied by one O_{ClO4^-} donor with a $Cu-O_{ClO4^-}$ distance of 2.394 Å, which is longer than the Cu-N distance (2.000 Å) on the equatorial

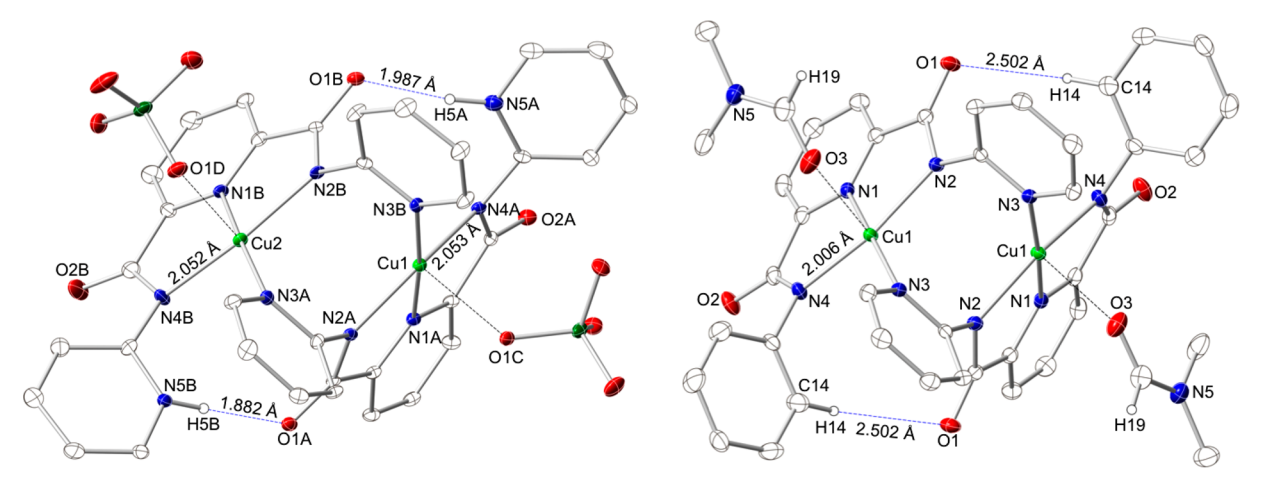


Figure 1. X-ray structures of complexes 1 (left) and 2 (right). Thermal ellipsoids are shown at the 30% probability level. Most hydrogen atoms are omitted for clarity. See Table 1 for selected bond lengths and angles.

Table 1. Selected Bond Lengths (Å) and Angles (deg) of Complexes 1 and 2

complex 1				complex 2	
Cu1-N1A	1.943(5)	Cu1-N1B	1.934(5)	Cu1-N1	1.9209(17)
Cu1-N3B	1.974(5)	Cu1-N3A	1.985(5)	Cu1-N3	1.9630(17)
Cu1-N2A	2.028(5)	Cu1-N2B	2.029(6)	Cu1-N2	2.0356(15)
Cu1-N4A	2.053(5)	Cu1-N4B	2.050(6)	Cu1-N4	2.0063(17)
Cu1-O1C	2.408(5)	Cu1-O1D	2.380(5)	Cu1-O3	2.5774(16)
Cu···Cu	3.627			Cu···Cu	3.586
N1A-Cu1-N3B	173.7(2)	N1B-Cu2-N3A	173.0(2)	N1-Cu1-N3	172.22(7)
N1A-Cu1-N2A	79.9(2)	N1B-Cu2-N2B	79.6(2)	N1-Cu1-N2	79.70(7)
N3B-Cu1-N2A	99.1(2)	N3A-Cu2-N2B	100.4(2)	N3-Cu1-N2	102.40(7)
N1A-Cu1-N4A	80.3(2)	N1B-Cu2-N4B	80.1(2)	N1-Cu1-N4	80.76(7)
N3B-Cu1-N4A	99.9(2)	N3A-Cu2-N4B	98.9(2)	N3-Cu1-N4	96.70(7)
N2A-Cu1-N4A	159.24(19)	N2B-Cu2-N4B	158.8(2)	N2-Cu1-N4	160.34(7)
N1A-Cu1-O1C	89.82(19)	N1B-Cu2-O1D	97.3(2)	N1-Cu1-O3	96.00(6)
N3B-Cu1-O1C	96.41(19)	N3A-Cu2-O1D	89.77(19)	N3-Cu1-O3	91.69(6)
N2A-Cu1-O1C	88.73(18)	N2B-Cu2-O1D	90.4(2)	N2-Cu1-O3	83.89(6)
N4A-Cu1-O1C	97.38(18)	N4B-Cu2-O1D	98.4(2)	N4-Cu1-O3	100.29(6)

positions. On the square-planar base, one N_{py} and two $N_{amidate}$ donors from one ligand embrace the Cu(II) center, and the fourth position is fulfilled by one N_{py} donor from the second ligand. Each ligand has one pyridinium group, suggesting a proton migration during the metalation of the ligand. As a result, two intramolecular hydrogen-bonding interactions are observed in the X-ray crystal structure (blue dashed lines in Figure 1, left). This can be confirmed by Hirshfeld surface analysis based on half of the dimeric unit, in which two distinct red dots are clearly observed on the map plotted by d_{norm} (Figure S1). The Cu···Cu distance is 3.627 Å, suggesting no direct interaction between the two copper centers. Fiedler et al. reported a similar dimeric structure, in which the Cu(II) centers are supported by H_2 bpda derivative ligands and OTfanions.

In our effort to better understand the function of the terminal pyridyl groups on the amine side of the symmetric ligand H₂bpda, the copper chemistry of the unsymmetric ligand H₂ppda was investigated so that the coordination behavior of both ligands could be compared. Instead of having two pyridyl groups on both amide arms, the ligand H₂ppda features one phenyl group and one pyridyl group. We envisioned that this ligand with fewer coordination donors in

an unsymmetrical arrangement might lead to an interesting change in the coordination environment and second coordination sphere. The reaction of neutral H₂ppda with Cu(OAc)₂ in DMF resulted in the formation of a similar dinuclear Cu(II) complex (Figure 1 right). However, due to the lower denticity of H₂ppda, interesting structural differences were observed. (a) In both complexes, intramolecular hydrogen-bonding interactions occur at similar positions (N5B-H5B···O1A/N5A-H5A···O1B in complex 1 and C14-H14···O1 in complex 2), but the strengths are very different, which is reflected by the much shorter N···O distances in complex 1 (2.772 and 2.794 Å) in comparison to the C···O distance of complex 2 (3.367 Å) (Table 1). (b) As a result of the stronger intramolecular hydrogen-bonding interactions in complex 1, the amide groups containing hydrogen bond donors (O1A and O1B) present larger twist angles (71.79 and 75.05°) with the coordinated pyridyl groups in comparison to complex 2 (58.77°). In the meantime, the Cu···Cu distance in complex 1 (3.627 Å) is slightly larger than that of complex 2 (3.586 Å). (c) The Cu1-N4A (2.053 Å) and Cu2-N4B (2.052 Å) distances in complex 1 are longer than the Cu1-N4 distance (2.006 Å) in complex 2. This could be attributed to the greater π -conjugation effect involved in the

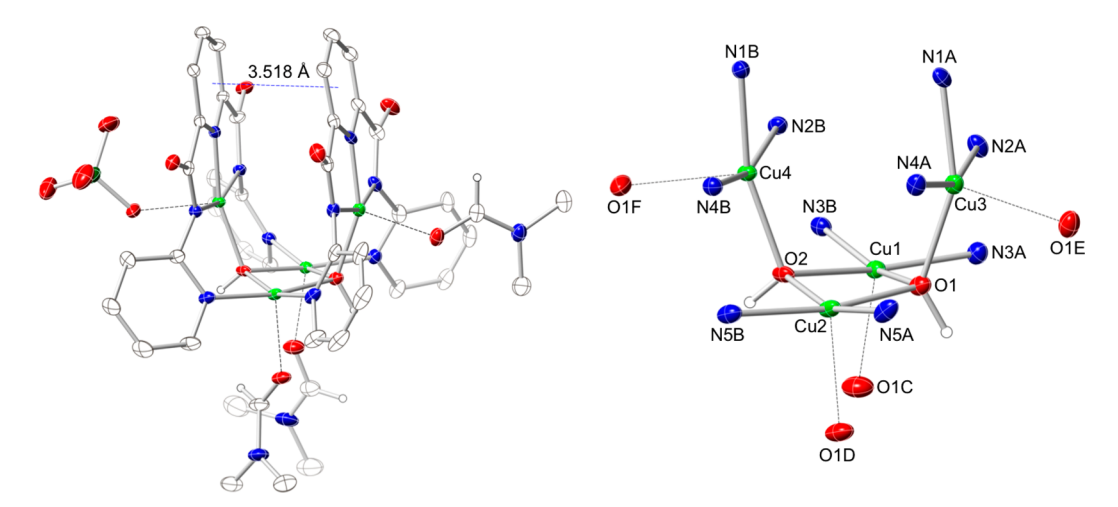


Figure 2. (left) X-ray structure of the cationic unit $[Cu^{II}_4(bpda)_2(\mu_3-OH)_2(ClO_4)(DMF)_3]^+$ of complex 3. (right) Core structure of the cationic unit without the ligand backbone. Thermal ellipsoids are shown at the 30% probability level. Most hydrogen atoms are omitted for clarity. See Table 2 for selected bond lengths and angles.

pyridinium-amide side arm in complex 1 (Figure S2). Among the three resonance structures of Hbpda-, two structures present a neutral imine group, which provides a weaker σ N donor. For the two resonance structures of ppda²⁻, only one shows a neutral imine N donor. Therefore, the overall greater neutral nature of the N donor in the ligand Hbpda may result in a weaker Cu-N bond. (d) Both complexes show elongated Cu-O bonds on the axial positions of copper centers, but the Cu-O_{ClO4} bond (2.394 Å) in complex 1 is significantly shorter than the Cu-O_{DMF} bond (2.577 Å) in complex 2. This could be attributed to the better attraction between ClO₄anions and the cationic $[Cu_2(Hbpda)_2]^{2+}$ unit in complex 1. However, in complex 2, neutral DMF molecules just interact weakly with copper centers of the neutral [Cu₂(ppda)₂] unit. In order to better understand the conformation difference, a graphical overlay of ligands with copper centers from both complexes is shown in Figure S3. The central motif (middle pyridyl group, copper center, and the two amide groups) of both complexes are superposed nearly perfectly, but the terminal pyridyl and phenyl groups have very different spatial orientations, largely due to the free rotation of N_{amide}-C bonds.

For complex 1, the self-deprotonation and proton migration of the neutral ligand H₂bpda led to the formation of a dimeric structure with interesting intramolecular hydrogen-bonding interactions involving pyridinium groups. On the basis of this work, we envisioned the potential nitrogen donors of pyridinium groups under basic conditions might be able to afford copper clusters with higher nuclearity, which is one of our main focuses in the model chemistry of copper-containing enzymes. Therefore, as part of our effort to explore the coordination behavior of the fully deprotonated ligands, we also used the organic base Et₃N to react with ligands before metalation. Complex 3 was synthesized by mixing the ligand H₂pbda and excess Et₃N in CH₃OH, followed by addition of Cu(ClO₄)₂·6H₂O. Recrystallization of the raw product in DMF gave dark green crystals, which are very moisture sensitive. X-ray crystallographic analysis revealed the tetranuclear copper cluster (HNEt₃)[$Cu^{II}_{4}(bpda)_{2}(\mu_{3}-OH)_{2}(ClO_{4})$ -(DMF)₃](ClO₄)₂ with a saddle-shaped conformation (Figure 2, left). In the outer sphere, there are two ClO₄⁻ anions and one Et₃NH cation to balance the charge of the complex. For

the core structure shown in Figure 2, right, there is a C_2 rotation axis that is perpendicular to the Cu1-O1-Cu2-O2 diamond core. Each of the two fully deprotonated pbda²⁻ ligands embraces one copper center (Cu3 and Cu4) through the middle pyridyl N and two $N_{amidate}$ donors. The two terminal pyridyl N donors of each ligand bind the other two copper centers (Cu1 and Cu2), which form a diamond core with two μ_3 -OH ligands (O1 and O3 in Figure 2, right). It is noticeable that the average Cu-N bond distance in complex 3 (1.985 Å) is shorter than that of complex 1 (2.008 Å). This could be attributed to the coordination of both terminal pyridyl groups in complex 3, making the core structure more rigid. All of the four copper centers have a square-pyramidal geometry with an elongated Cu-O bond on the axial position. However, the Cu4 center with a ClO₄⁻ anion has a much smaller au_5 value $(0.0080)^{50}$ in comparison to the other three copper centers $(\tau_5 = 0.063 - 0.097)^{50}$ with DMF molecules, suggesting a structure closer to a standard square-pyramidal geometry. This is attributed to the $Cu-O_{ClO4}^-$ distance (2.456 Å) of Cu4 being much longer than the Cu-O_{DMF} distances (2.196–2.228 Å) of the other three copper centers, resulting in a better square-planar base of Cu4 (Table 2). This elongation difference is exactly opposite to that observed from complexes 1 and 2, in which the $Cu-O_{ClO4}$ distance (2.394 Å) is shorter

Table 2. Selected Bond Lengths (Å) and Angles (deg) of Complex 3

Cu1-O1	1.981(6)	Cu3-N1A	1.920(6)
Cu1-N3B	1.990(6)	Cu3-O1	1.973(5)
Cu1-N3A	2.0916(16)	Cu3-N2A	2.012(5)
Cu1-O2	2.001(5)	Cu3-N4A	2.023(5)
Cu1-O1C	2.228(6)	Cu3-O1E	2.196(6)
Cu2-O1	1.977(5)	Cu4-N1B	1.908(6)
Cu2-N5B	1.996(7)	Cu4-O2	1.930(5)
Cu2-N5A	1.998(8)	Cu4-N2B	2.003(5)
Cu2-O2	2.003(6)	Cu4-N4B	2.017(5)
Cu2-O1D	2.209(5)	Cu4-O1F	2.456(6)
O1-Cu1-N3B	163.8(2)	N1A-Cu3-O1	154.3(2)
N3A-Cu1-O2	167.6(3)	N2A-Cu3-N4A	159.6(3)
O1-Cu2-N5B	168.4(2)	N1B-Cu4-O2	162.5(3)
N5A-Cu2-O2	162.6(2)	N2B-Cu4-N4B	162.0(2)

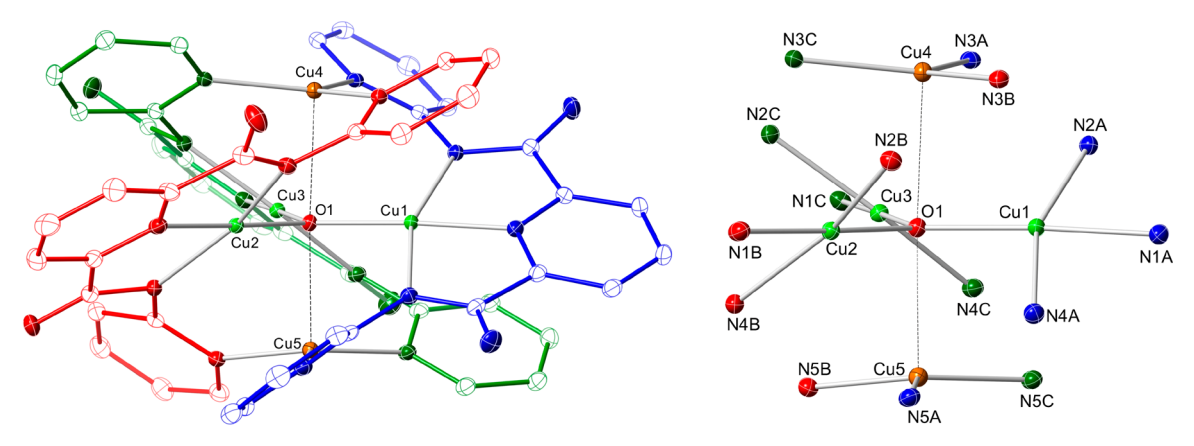


Figure 3. (left) X-ray structure of complex 5. (right) Core structure without the ligand backbone. Thermal ellipsoids are shown at the 30% probability level. Hydrogen atoms are omitted for clarity. See Table 3 for selected bond lengths and angles.

than the Cu-O_{DMF} distance (2.577 Å). The reason for the much shorter Cu-O_{DMF} distance in complex 3 could be the involvement of the three coordinated DMF molecules in a complicated hydrogen-bonding network, which locks these DMF molecules into close interactions with the copper centers (blue dashed lines in Figure S4). Among the observed hydrogen-bonding interactions, two interactions involving both μ_3 -OH and two DMF molecules are quite distinctive. The short O_{OH}···O_{DMF} distances (2.648 and 2.662 Å) indicate the strong interactions between the acceptor and donor. Hirshfeld analysis of the two DMF molecules revealed two intense red dots (green circles in Figure S5, left) on the surface mapped with d_{norm} , indicating the presence of strong hydrogenbonding interactions. The second type of noncovalent interaction observed in complex 3 is the $\pi \cdots \pi$ stacking interaction between the two middle pyridyl groups that are parallel to each other with a centroid to centroid distance of 3.518 Å. In fact, the Hirshfeld surface of one ligand plotted by the surface index shows a distinctive blue-red triangle pair (red circle in Figure S5, right), strongly suggesting the presence of intramolecular $\pi \cdots \pi$ interactions. The involvement of DMF molecules in the first and second coordination spheres of complex 3 explains why the raw product from CH₃OH dissolves well in DMF and the recrystallization trials in other non-coordinating or weakly coordinating solvents did not lead to any positive results.

The tetranuclear cluster of complex 3 inspired us to use the ligand H₂ppda to explore how the unsymmetrical ligand donor arrangement affects the structures of the resulting complexes. With the application of 2 equiv of Et₃N, the reaction of H_2 ppda and $Cu(ClO_4)_2 \cdot 6H_2O$ in CH_3OH afforded complex 4. Synthesis with excess Et₃N led to the formation of the same product, suggesting the high stability of complex 4. Although the X-ray diffraction data of complex 4 have some disorder problems, a raw structure was obtained and is shown in Figure S6. The metallamacrocyclic structure has six copper centers connected by six deprotonated ppda²⁻ ligands through a headto-tail fashion. For each ligand, the middle pyridyl nitrogen and the two amidate nitrogen donors embrace one Cu(II) center and the carbonyl oxygen from the amide side arm with the terminal pyridyl group bridges to another Cu(II) center, serving as the fourth ligand donor that is trans to the middle pyridyl nitrogen donor. The Cu1 and Cu3 centers possess a distorted-square-pyramidal geometry with either a CH3OH molecule or H₂O molecule occupying the axial position.

Although both Cu–O bonds are elongated, Cu3– O_{H_2O} (2.460 Å) is slightly longer than $Cu1-O_{CH_3OH}$ (2.312 Å) possibly because of the hydrogen-bonding interactions of the H₂O molecules with the outer-sphere ClO₄⁻ anion. The Cu2 center has a distorted-square-planar geometry with a τ_4 value of 0.162.⁵² The lack of a fifth ligand on the Cu2 center is quite intriguing, especially considering the presence of outer-sphere H₂O molecules and ClO₄⁻ anions. A close inspection of the crystal structure shows some interesting structural features of the Cu2 center. (a) A phenyl ring from the ligand neighboring the Cu3 center sits above the square-planar Cu2 center with a closest Cu···C distance of 4.316 Å, which may block the access of the fifth ligand. (b) A pendant pyridyl ring from the ligand neighboring the Cu1 center sits below the Cu2 center with a closest Cu···C distance of 2.912 Å. Although this distance is too long for any bonding interactions, Hirshfeld analysis based on the pendant pyridyl ring indicates the presence of weak interactions between Cu2 and the aromatic carbon on the pyridyl ring. The plot mapped with shape index (Figure S7, left) clearly shows a red spot on the surface, representing the concave region caused by the Cu2 center. Although this interaction could not be reflected by the surface mapped with d_{norm} , the fingerprint plot shows the Cu···C interaction comprises 3.5% of the total surface, suggesting very weak interactions (Figure S7, right).

Other interesting structural features of complex 4 are the positions of the pyridyl groups and pendant phenyl of the six ligands (Figure S8, left). Above and below the macrocyclic structure, there are three pyridyl groups on each side pointing inward (blue and red). These three pyridyl groups take on a triangle conformation, with a ~48.1° angle between two pyridyl planes. This organized conformation is attributed to the C-H··· π interactions between pyridyl rings (blue and red dashed lines, average C-H···centroid distance 3.23 Å), which can be confirmed by the intermolecular complementarity on the Hirshfeld surface mapped with shape index (Figure S8, right). The red spot (red circle) and blue spot (green circle) represent the concave region (acceptor, close to the center of the pyridyl ring) and convex region (donor, H on pyridyl ring pointing to another pyridyl group), respectively, from the same pyridyl ring. For all of the six phenyl rings (black) sitting outside the metallacycle, they are pointed away from the center and exhibit disorder possibly due to the lack of significant intermolecular interactions.

In our previous work, delocalized mixed-valence copper clusters were prepared by using the simple dipyridylamide ligand H₂pcp. ²⁹ The interesting coordination behavior exhibited by ligands H₂pbda and H₂ppda in Cu(II) chemistry shows us their potential in the construction of mixed-valence copper clusters, which is one of the main focuses of our research. Our initial effort on the mixed-valence chemistry of the ligand H₂pbda afforded the pentanuclear mixed-valence cluster complex 5, which is an unexpected product with a very low yield (~10%) due to the trace amount of water in DMF. We believe the H₂O molecules are deprotonated by an excess amount of NaH, leading to the formation of a μ_3 -oxo bridging ligand among copper centers. Therefore, a modified synthesis with the addition of degassed water in a 1:1.5 H₂O:Cu stoichiometry ratio and excess NaH was performed, resulting in the same product with a much better yield (52%) and higher quality crystals. X-ray crystallographic analysis revealed a novel pentanuclear cluster that has a three-bladed propeller conformation with a triple-decker core structure (Figure 3)

The pentanuclear structure of complex 5 consists of three deprotonated pbda2- ligands (highlighted in red, blue, and green in Figure 3, left), three Cu(II) centers, two Cu(I) centers, and one μ_3 -oxo bridging ligand. Cu1, Cu2, and Cu3 centers show a typical Cu(II) square-planar geometry (average $\tau_{\rm a} = 0.167)^{52}$ with a N₃O coordination environment. Each $pbda^{2-}$ ligand embraces one Cu(II) center through the middle pyridyl N donor and two amidate N donors with an average Cu-N bond length of 2.043 Å. The fourth position of the Cu(II) centers is occupied by the μ_3 -oxo bridging ligand that is trans to the middle pyridyl N donor. The trigonal-planar geometry of the μ_3 -oxo ligand has an average Cu(II)-O bond distance of 1.894 Å and an average Cu(II)-O-Cu(II) bond angle of 119.9° , suggesting an $s\bar{p}^2$ configuration of the oxo ligand (Table 3). The two Cu(I) centers Cu4 and Cu5 sit right above and below the μ_3 -oxo center, forming a Cu(I)-O-Cu(I) C_3 rotation axis of the whole structure. The average Cu(I)···O distance is 2.355 Å, suggesting a weak interaction

Table 3. Selected Bond Lengths (Å) and Angles (deg) of Complex 5

Cu1-O1	1.8981(13)	Cu3-N2C	2.0940(16)
Cu1-N1A	1.9357(16)	Cu3-O1	1.8935(13)
Cu1-N4A	2.0916(16)	Cu4-N3A	2.0029(16)
Cu1-N2A	2.0981(16)	Cu4-N3C	2.0084(16)
Cu2-O1	1.8907(13)	Cu4-N3B	2.0116(16)
Cu2-N1B	1.9345(16)	Cu5-N5C	2.0033(16)
Cu2-N2B	2.0937(16)	Cu5-N5A	2.0060(17)
Cu2-N4B	2.1088(16)	Cu5-N5B	2.0137(16)
Cu3-N1C	1.9360(16)	Cu4···O1	2.4048(13)
Cu3-N4C	2.0906(16)	Cu5···O1	2.3040(13)
O1-Cu1-N1A	176.74(6)	O1-Cu3-N1C	178.94(6)
O1-Cu1-N4A	99.66(6)	O1-Cu3-N4C	100.25(6)
N1A-Cu1-N4A	79.22(7)	N1C-Cu3-N4C	79.49(7)
O1-Cu1-N2A	101.70(6)	O1-Cu3-N2C	100.92(6)
N1A-Cu1-N2A	79.35(7)	N1C-Cu3-N2C	79.33(7)
N4A-Cu1-N2A	158.56(6)	N4C-Cu3-N2C	158.82(6)
O1-Cu2-N1B	177.47(6)	N3A-Cu4-N3C	119.06(7)
O1-Cu2-N2B	101.51(6)	N3A-Cu4-N3B	122.64(7)
N1B-Cu2-N2B	79.69(7)	N3C-Cu4-N3B	117.68(7)
O1-Cu2-N4B	99.60(6)	N5C-Cu5-N5A	122.39(7)
N1B-Cu2-N4B	79.22(7)	N5C-Cu5-N5B	118.10(7)
N2B-Cu2-N4B	158.88(6)	N5A-Cu5-N5B	117.37(7)

between the Cu(I) and the μ_3 -oxo ligand. The Hirshfeld surface plotted based on d_{norm} of the μ_3 -oxo ligand shows light red dots toward the Cu(I) centers, confirming the presence of weak interactions (Figure S9). Each Cu(I) center forms a trigonal-planar geometry with three terminal pyridyl N donors from three pbda²- ligands. The average Cu(I)–N distance is 2.008 Å, and the average N–Cu(I)–N bond angle is 119.5°. Among the five copper centers, the average Cu(II)····Cu(II) and Cu(II)····Cu(I) distances are 3.309 and 3.021 Å, respectively, suggesting a localized mixed-valence copper cluster. In order to adapt to the triple-decker conformation, each ligand is tilted with a dihedral angle of 30° against the Cu^{II}₃O equatorial plane.

A close inspection of the intermolecular interaction between pentanuclear units showed the presence of strong C–H··· π interactions (blue dashed lines in Figure S10, left). The hydrogen atoms on the terminal pyridyl rings point to the terminal pyridyl rings from a neighboring pentanuclear unit with an average C–H···centroid distance of 2.864 Å. The Hirshfeld surface (Figure S10, right) mapped with shape index based on one terminal pyridyl ring shows the interaction of a donor (blue area with a green circle) and an acceptor (red area with a red circle). These intermolecular interactions organize pentanuclear units into a coaxial arrangement along the Cu(I)–O–Cu(I) C_3 rotation axis to form a one-dimensional polymeric structure (Figure S11).

DFT calculations were carried out on complex 5 to gain insights regarding the localized mixed-valence nature. The structure of the complex was first optimized with the M06-L functional (Table S2), followed by specific analysis to assign and explain the spectroscopic results. Population analysis and Cu 2p electron binding energies were used to justify the assignment of the localized mixed-valence state (class I or weakly coupled class II mixed valence) in the pentanuclear copper core of complex 5 that contains axial copper(I) and equatorial copper(II) centers. The axial and equatorial copper atoms exhibited distinct NBO atomic charges and Mulliken spin populations. The equatorial copper centers exhibit an average NBO charge of +1.04 and an average Mulliken spin corresponding to 0.54 unpaired electron each. The axial copper centers have an average charge of +0.76 and an average Mulliken spin corresponding to 0.082 unpaired electron each. These data are consistent with distinct Cu(I) and Cu(II) centers in the axial and equatorial positions, respectively.

UV-Vis and EPR. The UV-vis spectra of the five complexes were collected in solution and in the solid state in order to obtain geometry information and better understand the electronic structures of the copper centers (Table S3 and Figures S12-S14). In solution, complexes 1-4 show d-d bands in the region of 630-668 nm, which could be assigned as the $d_{z^2} \to d_{x^2-y^2}$ transitions of the five-coordinate geometries observed in crystal structures.^{53–57} The positions of these absorption maxima shift to higher energy in DMF due to the stronger interaction of DMF with copper centers on the axial positions. 54,58-60 In the solid state, the d-d bands of complexes 1 and 2 red-shift to lower energy positions, suggesting a weaker LFS in the solid state. In contrast, the d-d bands of complexes 3 and 4 blue-shift to higher energy positions in the solid state, indicating a stronger interaction between the ligand donor and copper centers. For complex 5, the transition band around 570 nm could be a mixture of Cu(II) d-d transition and charge transfer bands (see the following TD-DFT calculation discussion). The position of

this band matches with the d–d transitions of the previously reported copper complexes with a square-planar geometry 53,56 but has a higher energy than the d–d transition bands of complexes 1–4, which could be attributed to the stronger LFS of the coordinated ligands. This transition band only shifted slightly in CH₂Cl₂ and DMF and in the solid state, suggesting that the square-planar geometry is retained. After exposure to air, the solution UV–vis spectra of complex 5 only exhibited some minor changes (Figure S15). The band around 578 nm in CH₂Cl₂ shifts to 583 nm, but in DMF the band shifts to 608 nm, suggesting a coordination environment change after the oxidation of the copper center(s) with the presence of coordinating solvent molecules.

In order to better understand the electronic structure of complex 5, TD-DFT calculations were performed to examine the nature of the electron transitions. As discussed above, the UV-vis spectrum of complex 5 shows an intense absorption in the region between 500 and 600 nm, which is somewhat unusual for the d-d transition of the Cu(II) centers. Our calculations revealed a large density of states in the region of interest; therefore, a sampling of the most intense absorptions in the range of 500-600 nm were chosen for analysis (Figure S16). These excited states were difficult to analyze by inspection of their individual excitations, because most of them contained upward of 15 components that were not dominated by one excitation. Natural transition orbital analysis yielded similar results. To obtain a more qualitative understanding of the nature of these excited states, the TD-DFT transition difference densities were plotted (Figure 4). The

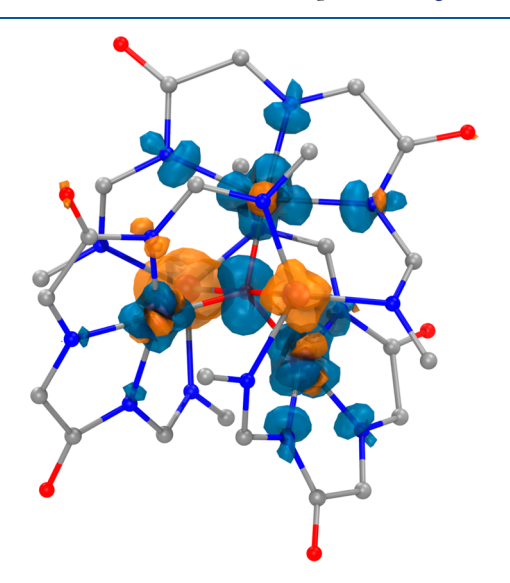


Figure 4. TD-DFT difference density plot for the calculated 528 nm excitation for the quartet state of complex **5.** Negative electron density differences (orange surface) and positive electron density differences (blue surface) are largely localized on the copper centers and their immediate ligand atoms. All hydrogen atoms and outer atoms on pyridyl rings have been omitted for clarity.

transitions in this region appear to have character that is dominated by axial $Cu(I) \rightarrow equatorial Cu(II)$ intermetallic charge transfer along with some Cu(II) d-d character. The presence of strong antiferromagnetic coupling in complex 5 raises the possibility of the open-shell doublet state contributing to the observed UV-vis spectrum (see Magnetic Measurements). TD-DFT calculations starting from the

broken-symmetry doublet state yield a similar spectrum. In addition, TD-DFT density difference analysis of the brokensymmetry excitations in the 500-600 nm region show that the excited states have the same origin as those obtained in the high-spin calculation. Although we did not observe any clearly defined bands in the near-IR region, our calculation regarding the lower energy electronic transitions of complex 5 did show a weak single-component excitation at around 1172 nm. This character is attributed to the intervalence charge transfer from Cu(I) to Cu(II) (Figure S17). It should be noted that there is little overlap between the hole-particle pair densities for this transition, suggesting that the mixed-valence nature of the compound is relatively weak. Furthermore, the bridging oxide ligand's ability to mediate a mixed-valence state is diminished by the fact that the axial and equatorial copper centers interact with orthogonal oxygen 2p orbitals.

In order to better understand the electronic structures and magnetic behavior of the copper complexes, X-band EPR of complexes 1–3 and 5 were collected in frozen solutions at 77 K. Unfortunately, no hyperfine signals were observed even when toluene was used for sample preparation. The broad isotropic signals of the four complexes are shown in Figure S18. The g values of the complexes fall in a range of 1.91–2.18 (Table 5), which provided some help with the magnetic data analysis.

Electrochemistry. Complex 1 shows an irreversible wave at E = -0.010 V vs Ag/AgCl with a scan rate of 100 mV/s, suggesting structure collapse when Cu(II) is reduced to Cu(I) (Figure S19, left). For complex 2, a sharp spike was observed around -0.10 V, which might be attributed to the generation of Cu(0) metal from the reduction of Cu(II) centers (Figure S19, right). In fact, a copper film was observed on the surface of the working electrode after scans. The electrochemical properties of complexes 3 and 4 are not well-defined by CV scanning in organic solvents. Both complexes showed multiple oxidation waves and one broad reduction wave, and they are difficult to assign due to the multinuclear nature of the compounds (Figure S20). The mixed-valence property of complex 5 can be identified from the CV characterization (Figures S21 and S22). Two irreversible waves were observed at E = 0.085 and 0.638 V vs Ag/AgCl, and they could be ascribed to the one-electron oxidation of one Cu(I) center to Cu(II) and one Cu(II) center to Cu(III), respectively. 13 In addition, one reversible wave appears at $E_{1/2} = -0.83 \text{ V} \left(\Delta E_{p} = -0.83 \text{ V} \right)$ 40 mV, $i_{pa}/i_{pc} \approx 1$; Figure S21, right), which shows no significant changes with different scan rates. This reversible behavior is attributed to the reduction of Cu(II) center(s) in the cluster to Cu(I). One irreversible wave was also observed at -1.295 V, which might be from the reduction of more Cu(II) center(s) to Cu(I) that leads to the collapse of the

MALDI-MS. All five copper complexes were characterized by MALDI-MS spectrometry without the application of a matrix. Figures S23–S25 show the experimental and simulated peaks for complexes 1–5. The spectrum of complex 3 shows a peak at m/z 920.2, suggesting a tetranuclear copper cluster with two ligands and two bridging ligands. For the other four complexes, peaks that correspond to smaller multinuclear copper fragments were observed due to the loss of either ligands or copper centers. One interesting observation in the MALDI-MS characterization of these copper clusters is the reduction of Cu(II) to Cu(I). For instance, the spectrum of complex 5 shows a fully reduced pentanuclear Cu(I) with two

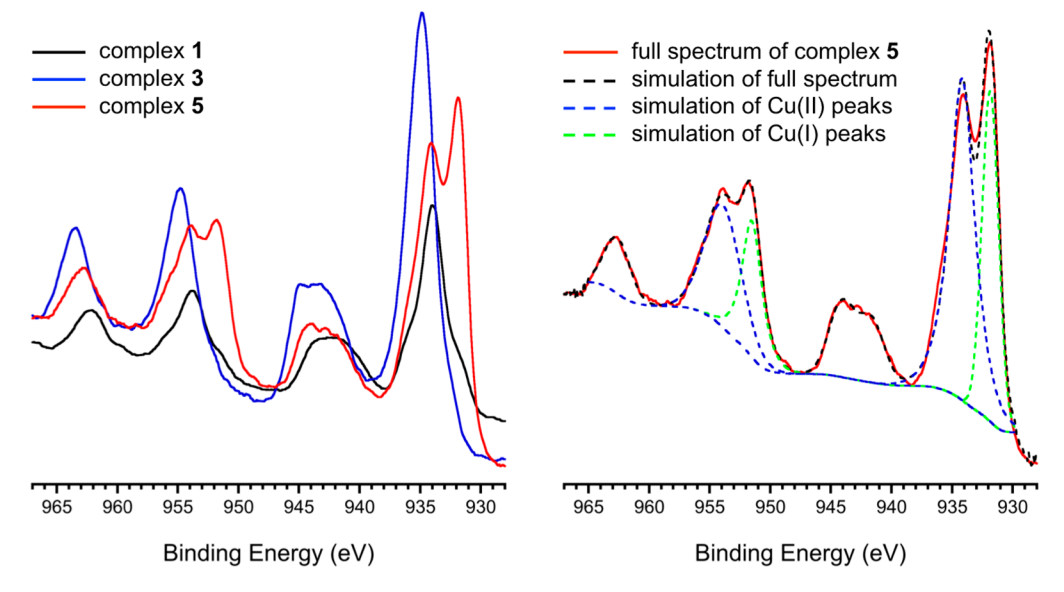


Figure 5. XPS spectra of complexes 1, 3, and 5 recorded in the Cu 2p region.

ppda $^{2+}$ ligands at m/z 951.1, which could be attributed to the reduction of the original $\mathrm{Cu^{II}}_3\mathrm{Cu^{I}}_2$ cluster. Previous studies of MALDI-MS of transition-metal complexes showed the reduction of metal centers due to either matrices as reducing agents or free electrons present in the MALDI plume. Since matrices were not used in our measurement, free electrons captured by copper center(s) might be the main reason for their reduction in the gas phase. In fact, a stainless steel metal plate was used as the sample well. Therefore, the free electron generated from photoelectric emission from analyte/metal plate interface could be the reason of the reduction phenomena. 62

XPS. In order to further characterize the mixed-valence nature of complex 5 and compare it with the fully oxidized Cu(II) clusters with the same ligand platform, XPS measurements were performed on complexes 1, 3, and 5 (Figure 5). For our analysis, the oxidation states of copper centers can be identified mainly by the binding energy of Cu 2p electrons. Table 4 summarizes the Cu $2p_{3/2}$, Cu $2p_{1/2}$, and O 1s binding

Table 4. Cu $2p_{3/2}$, Cu $2p_{1/2}$, and O 1s Binding Energies from XPS Measurements

	Cu 2p _{3/2} (eV)	Cu 2p _{1/2} (eV)	O 1s (eV)
complex 1	934.0	953.8	531.0
complex 3	934.9	954.8	532.2
complex 5	934.1 (Cu ^{II}) + 931.9 (Cu ^I)	953.9 (Cu ^{II}) + 951.8 (Cu ^I)	530.6

energy data of solid samples of the three complexes. Complex 1 exhibits Cu $2p_{3/2}$ and Cu $2p_{1/2}$ peaks at 934.0 and 953.8 eV, respectively, while Cu $2p_{3/2}$ and Cu $2p_{1/2}$ peaks of complex 3 shift to higher binding energy (934.9 and 954.8 eV), suggesting a lower atomic charge on the copper centers of complex 1. This is possibly due to the more electron rich coordination environment of the copper centers of complex 1 with more N as σ donors. For complex 5, the localized mixed-valence property is well featured by two sets of Cu 2p binding energy. The first set comes from the Cu(II) center with Cu $2p_{3/2}$ and Cu $2p_{1/2}$ peaks at 934.1 and 953.9 eV. This matches well with the Cu(II) 2p binding energy of complex 1, suggesting a

similar electron-rich coordination environment. The presence of satellites around 944.0 and 962.9 eV is possibly due to the p → d hybridization of unsaturated d orbitals, also indicating the presence of Cu(II) centers. 65 The second set at 931.9 and 951.8 eV comes from Cu(I) centers, which usually have lower Cu $2p_{3/2}$ and Cu $2p_{1/2}$ binding energy due to the lower oxidation state. 66 In our previous work on a Cu(I) dimer supported by H₂pcp ligands (Scheme 1), XPS showed nearly the same Cu $2p_{3/2}$ and Cu $2p_{1/2}$ binding energies (931.9 and 951.7 eV), which confirms the presence of Cu(I) centers. Detailed analysis by a peak-fitting procedure revealed the presence of two independent binding energies, separated by about 2.2 eV, from Cu(II) and Cu(I) centers in complex 5 (blue and green peaks in Figure 5, right). The relative abundance of Cu(II) and Cu(I) was also obtained as 61% and 39%, respectively, by calculation of the areas of two peaks. These analysis results are consistent with the localized mixedvalence property of complex 5 observed in X-ray crystallography. The interpretation of XPS data of complex 5 is also supported by DFT calculations. By examination of the calculated copper 2p orbitals, equatorial Cu(II) 2p orbital energies grouped into a set with an average of -922.236 eV. The axial Cu(I) 2p orbitals had weaker binding energies, with an average of -919.826 eV. This calculated difference of 2.41 eV in 2p binding energies between the two sites is a close match to the experimental value of 2.2 eV.

It is also worth noting that the O 1s binding energy shows an interesting trend (Figure S26). With O from C=O and ClO_4^- in complex 1, the O 1s binding energy is 531.0 eV. However, in complexes 3 and 5, the O 1s binding energies shift to 532.2 and 530.6 eV, respectively, possibly due to the presence of OH^- and O^{2-} ligands in the two complexes. A similar trend can also be observed from the reported O 1s binding energies of $Cu(OH)_2$ (531.5 eV) and CuO (529.5–530.7 eV). $^{67-71}$

Magnetic Measurements. The magnetic susceptibilities of complexes 1, 3, and 5 were measured as a function of temperature with a SQUID magnetometer between 2 and 300 K (Figure 6). Using the PHI software package, the magnetic susceptibilities of each complex were fit to a model Hamiltonian that included an electronic Zeeman component, the appropriate Heisenberg–Dirac–van Vleck exchange

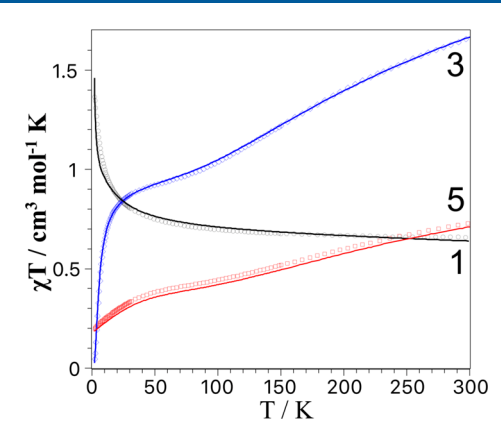


Figure 6. Overlaid plots of χT vs T for complexes 1 (black circles), 3 (blue circles), and 5 (red circles) along with fits of the data to the respective model Hamiltonians for complexes 1 (black line), 3 (red line), and 5 (blue line).

component, and an antisymmetric exchange component (vide infra) for complex 5. Each compound utilized the same Zeeman Hamiltonian that included isotropic g factors for each spin center, as shown in eq 1, with symmetrically related copper centers fit to the same g factor value:

$$H_{\text{ZEE}} = \mu_{\text{B}} \sum_{i=1}^{N} S_{i} g_{i} \cdot \overrightarrow{B}$$
 (1)

To improve the fitted values of the g factors in complexes 1 and 5, experimental EPR spectra were included in the data sets for these compounds. For each, the model Hamiltonian was formed through the simultaneous fitting of the model to both magnetic susceptibility and EPR data. Due to the presence of multiple Cu(II) centers in complex 3, the inclusion of the compound's broad, isotropic EPR spectrum in the data set degraded the quality of the fitting in comparison to the model formed using only the magnetic susceptibility data.

The magnetic behavior of complex 1 is consistent with a compound containing two weakly interacting Cu(II) centers, and the susceptibility fits well to a Curie–Weiss law at temperatures above 15 K (Figure 6). A positive deviation from linearity in the plot of χT vs T indicates behavior consistent with weak ferromagnetic coupling. This data was modeled with the Heisenberg–Dirac–van Vleck spin Hamiltonian in eq 2:

$$H_{\rm iso} = -2JS_1S_2 \tag{2}$$

The inclusion of EPR data allowed for the adequate fitting of the magnetic behavior of complex 1, which yielded g = 1.91 and J = 10.3 cm⁻¹ (Table 5), indicating relatively weak ferromagnetic exchange between the two copper(II) centers. Strong exchange coupling would not be expected in this complex due to the long Cu···Cu distance of 3.63 Å and lack of

a bridging ligand donor that can facilitate coupling. To adequately fit the magnetic susceptibility data below 20 K, it was necessary to include an intermolecular exchange coupling term, which added weak ($zJ = 0.22 \, \mathrm{cm}^{-1}$) ferromagnetic exchange between dinuclear Cu(II) units. Similar exchange constant values have been reported for dicopper(II) compounds that exhibit intra- and intermolecular ferromagnetic exchange.⁷²

The magnetic susceptibilities of complexes 3 and 5 exhibit significant deviations from Curie—Weiss behavior at temperatures below 150 K, suggesting stronger exchange coupling than what was observed in complex 1. The magnetic susceptibility of complex 3 descends to nearly 0 at low temperatures, indicating that antiferromagnetic coupling among the four Cu(II) centers leads to an S=0 ground state. When only the four copper centers and their immediate ligand atoms are considered, the core structure of complex 3 has approximate $C_{2\nu}$ symmetry with two distinct sets of copper atoms. As previously described, 73 exchange coupling between spin centers in a distorted-tetrahedral arrangement of metal centers can be treated as shown in Scheme 2. This geometric configuration leads to the isotropic exchange Hamiltonian used to fit the data within Phi (eq 3):

$$H_{iso} = -2J_{S}(S_{1}S_{2}) - 2J_{M}(S_{1}S_{3} + S_{1}S_{4} + S_{2}S_{3} + S_{2}S_{4})$$
$$-2J_{L}S_{3}S_{4}$$
(3)

The fit of the data confirms strong antiferromagnetic coupling between each of the copper centers (Table 5), with the greatest interaction ($J_S = 106 \text{ cm}^{-1}$) between the two copper centers with the di- μ_3 -oxo ligands (Cu1 and Cu2 in Figure 2).

The magnetic behavior of complex 5 indicates antiferromagnetic coupling between unpaired spins. A plot of $\mu_{\rm eff}$ vs T (Figure S27) shows that the high-spin, quartet state is not fully populated at room temperature. According to the equation $\mu_{\rm eff} = \sqrt{8\chi T}$, the room-temperature effective magnetic moment of 2.51 $\mu_{\rm B}$ falls short of the spin-only magnetic moment of 3.87 $\mu_{\rm B}/$ molecule for three unpaired electrons due to the antiferromagnetic coupling. Conversely, at the low-temperature region of the SQUID experiment, the effective magnetic moment value descends to 1.28 $\mu_{\rm B}/$ molecule, which is smaller than expected for an S=1/2 system.

DFT population analysis suggests that the unpaired spin density in complex 5 resides on the three equatorial Cu(II) centers and that the axial Cu(I) centers do not participate in the spin system (Figure 7). For the purposes of interpreting magnetic behavior, the system was simplified to a D_{3h} trigonal-planar structure of Cu(II) centers with a μ_3 -oxo ligand in the center. This geometric configuration leads to the isotropic HDVV exchange Hamiltonian for complex 5 shown in eq 4:

Table 5. Experimental Exchange Coupling Values for Complexes 1, 3, and 5

complex	$J_{\rm exp}~({\rm cm}^{-1})$	g	$G_z \left(\text{cm}^{-1} \right)^b$	TIP $(cm^3 mol^{-1})^c$	$zJ (cm^{-1})^d$
1	10.3	1.91		2.08×10^{-4}	0.22
3 ^a	$-106 (J_{\rm S})$	$g_1 = g_2 = 2.15$		1.09×10^{-3}	
	$-31 (J_{\rm M})$	$g_3 = g_4 = 2.22$			
	$-3.6 (J_{\rm L})$				
5	-87	2.10	15	-2.13×10^{-4}	

"See Scheme 2 for atomic and *J*-coupling constant naming scheme. ^bAntisymmetric exchange parameter. ^cTemperature-independent paramagnetism. ^dIntermolecular exchange parameter.

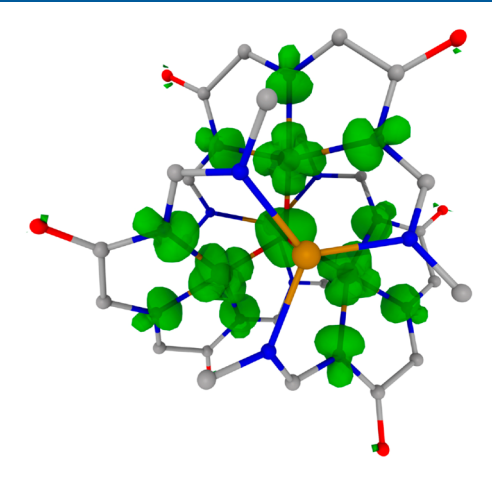


Figure 7. Unpaired spin density isosurface of complex 5 showing the localization of unpaired spin density on the equatorial copper centers and their immediate ligand atoms. All hydrogen atoms and outer atoms on pyridyl rings have been omitted for clarity.

$$H_{\rm iso} = -2J(S_1S_2 + S_1S_3 + S_2S_3) \tag{4}$$

However, the magnetic susceptibility fitting of complex 5 to the isotropic exchange Hamiltonian alone could not adequately account for the small χT values observed at temperatures below 40 K. Intermolecular antiferromagnetic exchange did not give a realistic explanation for this behavior because the center-to-center distance between molecular units is 8.2 Å. Furthermore, inclusion of a mean-field approximation term (zJ) into the model did not faithfully reproduce the line shape of the susceptibility at low temperatures.

As reported from previous studies in recent years, triangular spin systems such as those found in the equatorial copper(II) atoms of complex 5 have been of great interest because they exhibit geometric spin frustration. In these cases, the HDVV Hamiltonian is insufficient to explain the magnetic behavior, and therefore the additional inclusion of an antisymmetric exchange interaction (G_{ij}) between copper centers is necessary to fit the data. Treatment of the magnetic data of triangular Cu(II) complexes by including antisymmetric exchange is well-described in the literature. For an equilateral triangle arrangement of Cu(II) centers, the antisymmetric exchange Hamiltonian is shown in eq 5

$$H_{\text{ase}} = G_{12}(S_1 S_2) + G_{23}(S_2 S_3) + G_{31}(S_3 S_1)$$
 (5)

in which S_iS_j is the vector product and G_{ij} is the antisymmetric vector for which $G_{ij} = -G_{ji}$. Assuming that the system possesses D_{3h} symmetry, the vectors in eq 5 are identical, and only the component perpendicular to the equilateral triangle plane (G_z) is nonzero. This allows the antisymmetric exchange Hamiltonian to be simplified to the form shown in eq 6

$$H_{\text{ase}} = G_z(S_1 S_2 + S_2 S_3 + S_3 S_1) \tag{6}$$

leading to the inclusion of only one additional fitted parameter with respect to the exchange-coupling-only model Hamiltonian. The fit of the data confirms strong antiferromagnetic coupling in the trinuclear Cu(II) system ($J = -87 \text{ cm}^{-1}$) with an antisymmetric exchange parameter of 15 cm⁻¹ (Table 5). These values are consistent with those previously reported for triangular copper(II) compounds. In particular, the ratio of the two constants (-G/J) found for complex 5 (0.22) is in the range reported for compounds of this type (0.10–0.25).⁷⁶

CONCLUSION

X-ray crystallography and spectroscopy characterization showed that the pyridylamide ligands H₂bpda and H₂ppda are excellent supporting platforms for Cu(II) clusters (complexes 1-4) and a mixed-valence copper cluster (complex 5). The interesting dinuclear, tetranuclear, and hexanuclear structures of complexes 1-4 demonstrated that change of ligand coordination donors and reaction conditions can collaboratively influence the structural conformations of the resulting complexes. Structural and XPS evidence demonstrated the localized mixed-valence property of the pentanuclear copper complex 5. An investigation of the magnetic properties of complexes 1, 3, and 5 showed either weak ferromagnetic (complex 1) or antiferromagnetic coupling (complexes 3 and 5) among copper centers. Due to the triangular arrangement of the Cu(II) centers in complex 5, an antisymmetric exchange interaction was required to better interpret its magnetic behavior. DFT calculations rationalized the UV-vis and XPS features of these complexes. For complex 5, unpaired spin density isosurface calculations show that the unpaired spin density resides on the equatorial copper(II) centers. This evidence supports the conclusion from spectroscopic characterization regarding the localized mixedvalence feature of the cluster.

ASSOCIATED CONTENT

Supporting Information

CCDC 1905176–1905178 (complexes 1-3) and 1905180 (complex 5) contain the supplementary crystallographic data. These data can be obtained free of charge from the Cambridge Crystallographic Data Centre via www.ccdc.cam.ac.uk/data_request/cif. The Supporting Information is available free of charge at https://pubs.acs.org/doi/10.1021/acs.inorg-chem.0c000008.

Spectroscopic data, cyclic voltammetry, Hirschfeld surfaces, MALDI-MS and X-ray crystallographic data, and details of the calculations (PDF)

Accession Codes

CCDC 1905176–1905178 and 1905180 contain the supplementary crystallographic data for this paper. These data can be obtained free of charge via www.ccdc.cam.ac.uk/data_request/cif, or by emailing data_request@ccdc.cam.ac.uk, or by contacting The Cambridge Crystallographic Data Centre, 12 Union Road, Cambridge CB2 1EZ, UK; fax: +44 1223 336033.

AUTHOR INFORMATION

Corresponding Authors

Gerard T. Rowe — Department of Chemistry & Physics, University of South Carolina—Aiken, Aiken, South Carolina 29801, United States; orcid.org/0000-0002-7935-8034; Email: gerardr@usca.edu

Lei Yang — Department of Chemistry, University of Central Arkansas, Conway, Arkansas 72035, United States;
o orcid.org/0000-0002-9936-9435; Email: lyang@uca.edu;
Fax: +1(501)4503623

Authors

Joseph D. Schneider — Department of Chemistry, University of Central Arkansas, Conway, Arkansas 72035, United States Brett A. Smith — Department of Chemistry & Physics, University of South Carolina—Aiken, Aiken, South Carolina 29801, United States

Grant A. Williams – Department of Chemistry, University of Central Arkansas, Conway, Arkansas 72035, United States

Douglas R. Powell – Department of Chemistry and Biochemistry, University of Oklahoma, Norman, Oklahoma 73019, United States

Felio Perez – Integrated Microscopy Center, University of Memphis, Memphis, Tennessee 38152, United States

Complete contact information is available at: https://pubs.acs.org/10.1021/acs.inorgchem.0c00008

Notes

The authors declare no competing financial interest.

ACKNOWLEDGMENTS

This work was supported by the College of Natural Sciences and Mathematics (CNSM) and University Research Council (URC) from the University of Central Arkansas, Arkansas Science & Technology Authority (ASTA) from the State of Arkansas, and the NSF (RUI Grant 1856438). We thank INBRE of Arkansas for the purchase of an EPR instrument and the NSF (Grant CCLI 0125711) for the purchase of a glovebox. We also thank Dr. Nan Xu at Penn State University—Altoona for collecting the electrochemistry data of complex 4.

REFERENCES

- (1) Farrar, J. A.; Neese, F.; Lappalainen, P.; Kroneck, P. M. H.; Saraste, M.; Zumft, W. G.; Thomson, A. J. The Electronic Structure of Cu_A: A Novel Mixed-Valence Dinuclear Copper Electron-Transfer Center. *J. Am. Chem. Soc.* **1996**, *118*, 11501–11514.
- (2) Sekretaryova, A.; Jones, S. M.; Solomon, E. I. O₂ Reduction to Water by High Potential Multicopper Oxidases: Contributions of the T1 Copper Site Potential and the Local Environment of the Trinuclear Copper Cluster. *J. Am. Chem. Soc.* **2019**, *141*, 11304–11314.
- (3) Rasmussen, T.; Berks, B. C.; Sanders-Loehr, J.; Dooley, D. M.; Zumft, W. G.; Thomson, A. J. The Catalytic Center in Nitrous Oxide Reductase, Cu_z, Is A Copper-Sulfide Cluster. *Biochemistry* **2000**, 39, 12753–12756.
- (4) Ross, M. O.; MacMillan, F.; Wang, J.; Nisthal, A.; Lawton, T. J.; Olafson, B. D.; Mayo, S. L.; Rosenzweig, A. C.; Hoffman, B. M. Particulate Methane Monooxygenase Contains only Mononuclear Copper Centers. *Science* **2019**, *364*, 566–570.
- (5) Doerrer, L. H. Cu in Biology: Unleashed by O₂ and Now Irreplaceable. *Inorg. Chim. Acta* **2018**, 481, 4–24.
- (6) Vu, V. V.; Ngo, S. T. Copper Active Site in Polysaccharide Monooxygenases. Coord. Chem. Rev. 2018, 368, 134–157.
- (7) Trammell, R.; Rajabimoghadam, K.; Garcia-Bosch, I. Copper-Promoted Functionalization of Organic Molecules: from Biologically Relevant Cu/O₂ Model Systems to Organometallic Transformations. *Chem. Rev.* **2019**, *119*, 2954–3031.
- (8) Adam, S. M.; Wijeratne, G. B.; Rogler, P. J.; Diaz, D. E.; Quist, D. A.; Liu, J. J.; Karlin, K. D. Synthetic Fe/Cu Complexes: Toward Understanding Heme-Copper Oxidase Structure and Function. *Chem. Rev.* 2018, 118, 10840–11022.
- (9) Kochem, A.; Gennarini, F.; Yemloul, M.; Orio, M.; Le Poul, N.; Rivière, E.; Giorgi, M.; Faure, B.; Le Mest, Y.; Réglier, M.; Simaan, A. J. Simaan, Characterization of A Dinuclear Copper(II) Complex and Its Fleeting Mixed-Valent Copper(II)/Copper(III) Counterpart. ChemPlusChem 2017, 82, 615–624.
- (10) Gennarini, F.; David, R.; López, I.; Le Mest, Y.; Réglier, M.; Belle, C.; Thibon-Pourret, A.; Jamet, H.; Le Poul, N. Influence of Asymmetry on the Redox Properties of Phenoxo- and Hydroxo-Bridged Dicopper Complexes: Spectroelectrochemical and Theoretical Studies. *Inorg. Chem.* **2017**, *56*, 7707–7719.

- (11) Thibon-Pourret, A.; Gennarini, F.; David, R.; Isaac, J. A.; López, I.; Gellon, G.; Molton, F.; Wojcik, L.; Philouze, C.; Flot, D.; Le Mest, Y.; Réglier, M.; Le Poul, N.; Jamet, H.; Belle, C. Effect of Monoelectronic Oxidation of An Unsymmetrical Phenoxido-Hydroxido Bridged Dicopper(II) Complex. *Inorg. Chem.* **2018**, *57*, 12364–12375
- (12) Isaac, J. A.; Gennarini, F.; López, I.; Thibon-Pourret, A.; David, R.; Gellon, G.; Gennaro, B.; Philouze, C.; Meyer, F.; Demeshko, S.; Le Mest, Y.; Réglier, M.; Jamet, H.; Le Poul, N.; Belle, C. Room-Temperature Characterization of a Mixed-Valent $\mu\mu$ -Hydroxodicopper(II, III) Complex. *Inorg. Chem.* **2016**, 55, 8263–8266.
- (13) Halvagar, M. R.; Solntsev, P. V.; Lim, H.; Hedman, B.; Hodgson, K. O.; Solomon, E. I.; Cramer, C. J.; Tolman, W. B. Hydroxo-Bridged Dicopper(II, III) and (III, III) Complexes: Models for Putative Intermediates in Oxidation Catalysis. *J. Am. Chem. Soc.* **2014**, 136, 7269–7272.
- (14) Liu, L.; Wu, Y.; Wang, Z.; Zhu, J.; Zhao, Y. Mechanistic Insight into the Copper-Catalyzed Phosphorylation of Terminal Alkynes: A Combined Theoretical and Experimental Study. *J. Org. Chem.* **2014**, 79, 6816–6822.
- (15) Kafentzi, M. C.; Papadakis, R.; Gennarini, F.; Kochem, A.; Iranzo, O.; Le Mest, Y.; LePoul, N.; Tron, T.; Faure, B.; Jalila Simaan, A.; Réglier, M. Electrochemical Water Oxidation and Stereoselective Oxygen Atom Transfer Mediated by A Copper Complex. *Chem. Eur. J.* 2018, 24, 5213–5224.
- (16) Tao, W.; Bower, J. K.; Moore, C. E.; Zhang, S. Dicopper $\mu\mu$ -Oxo, $\mu\mu$ -Nitrosyl Complex from the Activation of NO or Nitrite at a Dicopper Center. *J. Am. Chem. Soc.* **2019**, *141*, 10159–10164.
- (17) Esmieu, C.; Orio, M.; Mangue, J.; Pécaut, J.; Ménage, S.; Torelli, S. Valence Localization at a Bio-inspired Mixed-Valent {Cu₂S}²⁺ Motif upon Solvation in Acetonitrile: Effect on Nitrous Oxide Reductase (N₂OR) Activity. *Chem. Eur. J.* **2018**, 24, 5060–5063.
- (18) Bagherzadeh, S.; Mankad, N. P. Oxidation of a $[Cu_2S]$ complex by N_2O and CO_2 : insights into a role of tetranuclearity in the Cu_Z site of nitrous oxide reductase. *Chem. Commun.* **2018**, *54*, 1097–1100.
- (19) Johnson, B. J.; Antholine, W. E.; Lindeman, S. V.; Graham, M. J.; Mankad, N. P. A One-hole Cu_4S Cluster with N_2O Reductase Activity: A Structural and Functional Model for Cu_2 . J. Am. Chem. Soc. **2016**, 138, 13107–13110.
- (20) Johnson, B. J.; Antholine, W. E.; Lindeman, S. V.; Mankad, N. P. A Cu₄S Model for the Nitrous Oxide Reductase Active Sites Supported Only by Nitrogen Ligands. *Chem. Commun.* **2015**, *51*, 11860–11863.
- (21) Bar-Nahum, I.; Gupta, A. K.; Huber, S. M.; Ertem, M. Z.; Cramer, C. J.; Tolman, W. B. Reduction of Nitrous Oxide to Dinitrogen by A Mixed Valent Tricopper-Disulfido Cluster. *J. Am. Chem. Soc.* **2009**, *131*, 2812–2814.
- (22) Esmieu, C.; Orio, M.; Torelli, S.; Le Pape, L.; Pecaut, J.; Lebrun, C.; Menage, S. N₂O Reduction at A Dissymmetric {Cu₂S}-containing Mixed-valent Center. *Chem. Sci.* **2014**, *5*, 4774–4784.
- (23) Esmieu, C.; Orio, M.; Ménage, S.; Torelli, S. Influence of Copper Coordination Spheres on Nitrous Oxide Reductase (N_2OR) Activity of A Mixed-Valent Copper Complex Containing a { Cu_2S } Core. *Inorg. Chem.* **2019**, 58, 11649–11655.
- (24) Lan, J.; Liao, T.; Zhang, T.; Chung, L. W. Reaction Mechanism of Cu(I)-Mediated Reductive CO_2 Coupling for the Selective Formation of Oxalate: Cooperative CO_2 Reduction To Give Mixed-Valence $Cu_2(CO_2^{\bullet})$ and Nucleophilic-Like Attack. *Inorg. Chem.* **2017**, 56, 6809–6819.
- (25) Cook, B. J.; Di Francesco, G. N.; Abboud, K. A.; Murray, L. J. Countercations and Solvent Influence CO₂Reduction to Oxalate by Chalcogen-Bridged Tricopper Cyclophanates. *J. Am. Chem. Soc.* **2018**, 140, 5696–5700.
- (26) McMoran, E. P.; Goodner, J. A.; Powell, D. R.; Yang, L. Synthesis and Characterization of Cu(II), Zn(II) and Fe(II) Complexes Supported by Pyridylamide Ligands. *Inorg. Chim. Acta* **2014**, *421*, 465–472.

- (27) Pauly, M. A.; Erwin, E. M.; Powell, D. R.; Rowe, G. T.; Yang, L. A Synthetic, Spectroscopic and Computational Study of Copper(II) Complexes Supported by Pyridylamide Ligands. *Polyhedron* **2015**, *102*, 722–734.
- (28) McMoran, E. P.; Dominguez, M. N.; Erwin, E. M.; Powell, D. R.; Rowe, G. T.; Yang, L. Structural Diversity, Spectral Characterization and Computational Studies of Cu(I) Complexes with Pyridylamide Ligands. *Inorg. Chim. Acta* **2016**, *446*, 150–160.
- (29) McMoran, E. P.; Powell, D. R.; Perez, F.; Rowe, G. T.; Yang, L. Synthesis and Characterization of Copper Complexes with Cu^ICu^I, Cu^{I.5}Cu^{I.5} and Cu^{II}Cu^{II} Core Structures Supported by A Flexible Dipyridylamide Ligand. *Inorg. Chem.* **2016**, *55*, 11462–11472.
- (30) Jain, S. L.; Bhattacharyya, P.; Milton, H. L.; Slawin, A. M.; Crayston, J. A.; Woollins, J. D. New Pyridine Carboxamideligands and Their Complexation to Copper(II). X-Ray Crystal Structures of Mono-, Di, Tri- and Tetranuclear Copper Complexes. *Dalton Trans.* **2004**, 862–871.
- (31) Data Collection: SMART Software Reference Manual; Bruker-AXS: Madison, WI, 1998. Data Reduction: SAINT Software Reference Manual; 1998, Bruker-AXS: Madison, WI, 1998.
- (32) Sheldrick, G. M. SHELXTL Version 6.10 Reference Manual; Bruker-AXS: Madison, WI, 2000.
- (33) International Tables for Crystallography; Kluwer: Boston, 1995; Vol. C, Tables 6.1.1.4, 4.2.6.8, and 4.2.4.2.
- (34) Wolff, S. K.; Grimwood, D. J.; McKinnon, J. J.; Turner, M. J.; Jayatilaka, D.; Spackman, M. A. University of Western Australia; available online at: www.hirshfeldsurface.net (accessed July 09, 2015).
- (35) Morrison, G.; zur Loye, H. C. Simple Correction for the Sample Shape and Radial Offset Effects on SQUID Magnetometers: Magnetic Measurements on Ln_2O_3 (Ln=Gd, Dy, Er) Standards. *J. Solid State Chem.* **2015**, 221, 334–337.
- (36) Chilton, N. F.; Anderson, R. P.; Turner, L. D.; Soncini, A.; Murray, K. S. PHI: A Powerful New Program for the Analysis of Anisotropic Monomeric and Exchange-coupled Polynuclear d- and f-block Complexes. *J. Comput. Chem.* **2013**, *34*, 1164–1175.
- (37) Neese, F. The ORCA Program System Wiley Interdisciplinary Reviews: Computational Molecular. *Wiley Interdiscip. Rev.: Comput. Mol. Sci.* **2012**, *2*, 73–78.
- (38) Humphrey, W.; Dalke, A.; Schulten, K. VMD-Visual Molecular Dynamics. *J. Mol. Graphics* **1996**, *14*, 33–38.
- (39) Stone, J. An Efficient Library for Parallel Ray Tracing and Animation. Master's Thesis, Computer Science Department, University of Missouri-Rolla, 1998.
- (40) Frisch, M. J.; Trucks, G. W.; Schlegel, H. B.; Scuseria, G. E.; Robb, M. A.; Cheeseman, J. R.; Scalmani, G.; Barone, V.; Mennucci, B.; Petersson, G. A.; Nakatsuji, H.; Caricato, M.; Li, X.; Hratchian, H. P.; Izmaylov, A. F.; Bloino, J.; Zheng, G.; Sonnenberg, J. L.; Hada, M.; Ehara, M.; Toyota, K.; Fukuda, R.; Hasegawa, J.; Ishida, M.; Nakajima, T.; Honda, Y.; Kitao, O.; Nakai, H.; Vreven, T.; Montgomery, J. A., Jr.; Peralta, J. E.; Ogliaro, F.; Bearpark, M.; Heyd, J. J.; Brothers, E.; Kudin, K. N.; Staroverov, V. N.; Kobayashi, R.; Normand, J.; Raghavachari, K.; Rendell, A.; Burant, J. C.; Iyengar, S. S.; Tomasi, J.; Cossi, M.; Rega, N.; Millam, J. M.; Klene, M.; Knox, J. E.; Cross, J. B.; Bakken, V.; Adamo, C.; Jaramillo, J.; Gomperts, R.; Stratmann, R. E.; Yazyev, O.; Austin, A. J.; Cammi, R.; Pomelli, C.; Ochterski, J. W.; Martin, R. L.; Morokuma, K.; Zakrzewski, V. G.; Voth, G. A.; Salvador, P.; Dannenberg, J. J.; Dapprich, S.; Daniels, A. D.; Farkas, Ö.; Foresman, J. B.; Ortiz, J. V.; Cioslowski, J.; Fox, D. J. Gaussian 09, Revision C.01; Gaussian, Inc.: Wallingford, CT, 2009.
- (41) Zhao, Y.; Truhlar, D. The M06 Suite of Density Functionals for Main Group Thermochemistry, Thermochemical Kinetics, Noncovalent Interactions, Excited States, and Transition Elements: Two New Functionals and Systematic Testing of Four M06-class Functionals and 12 Other Functionals. *Theor. Chem. Acc.* 2008, 120, 215–241.
- (42) Weigend, F.; Ahlrichs, R. Balanced Basis Sets of Split Valence, Triple Zeta Valence and Quadruple Zeta Valence Quality for H to Rn: Design and Assessment of Accuracy. *Phys. Chem. Chem. Phys.* **2005**, *7*, 3297–3305.

- (43) Weigend, F. Accurate Coulomb-fitting Casis Sets for H to Rn. *Phys. Chem. Chem. Phys.* **2006**, *8*, 1057–1065.
- (44) Grimme, S.; Ehrlich, S.; Goerigk, L. Effect of the Damping Function in Dispersion Corrected Density Functional Theory. J. Comput. Chem. 2011, 32, 1456–1465.
- (45) Grimme, S.; Antony, J.; Ehrlich, S.; Krieg, H. A Consistent and Accurate Ab Initio Parametrization of Density Functional Dispersion Correction (DFT-D) for the 94 Elements H-Pu. *J. Chem. Phys.* **2010**, 132, 154104.
- (46) Kruse, H.; Grimme, S. A Geometrical Correction for the Inter and Intra-Molecular Basis Set Superposition Error in Hartree-Fock and Density Functional Theory Calculations for Large Systems. *J. Chem. Phys.* **2012**, *136*, 154101.
- (47) Wachters, A. J. H. Gaussian Basis Set for Molecular Wavefunctions Containing Third-Row Atoms. *J. Chem. Phys.* **1970**, 52, 1033–1036.
- (48) The ORCA basis set "CoreProp" was used. This basis set is based on the TurboMole DZ basis developed by Ahlrichs and coworkers along with polarization functions obtained from the TurboMole basis set library, available at https://cosmologic-services.de/basis-sets/basissets.php.
- (49) Neese, F.; Wennmohs, F.; Hansen, A.; Becker, U. Efficient, approximate and parallel Hartree-Fock and hybrid DFT calculations. A' 'chain-of-sphere' 's' algorithm for the Hartree-Fock exchange. *Chem. Phys.* **2009**, *356*, 98–109.
- (50) Addison, A. W.; Rao, T. N.; Reedjik, J.; Van Rijin, J.; Verschoor, G. C. Synthesis, Structure, and Spectroscopic Properties of Copper(II) Compounds Containing Nitrogen—sulphur Donor Ligands; the Crystal and Molecular Structure of Aqua[1,7-bis(N-methylbenzimidazol-2'-yl)-2,6-dithiaheptane]copper(II) Perchlorate. *J. Chem. Soc., Dalton Trans.* 1984, 1349—1356.
- (51) Wang, D.; Lindeman, S. V.; Fiedler, A. T. Intramolecular Hydrogen Bonding in Cu^{II} Complexes with 2,6-Pyridinedicarboxamide Ligands: Synthesis, Structural Characterization, and Physical Properties. *Eur. J. Inorg. Chem.* **2013**, 2013, 4473–4484.
- (52) Yang, L.; Powell, D. R.; Houser, R. P. Structural Variation in Copper(I) Complexes with Pyridylmethylamide Ligands: Structural Analysis with A New Four-coordinate Geometry Index, τ_4 . Dalton Trans. 2007, 955–964.
- (53) Matovic, Z. D.; Miletic, V. D.; Samardzic, G.; Pelosi, G.; Ianelli, S.; Trifunovic, S. Square-planar copper(II) complexes with tetradentate amido-carboxylate ligands. Crystal structure of Na₂[Cu-(obap)]₂·2H₂O. Strain analysis and spectral assignments of complexes. *Inorg. Chim. Acta* **2005**, 358, 3135–3144.
- (54) Lal, T. K.; Gupta, R.; Mahapatra, S.; Mukherjee, R. Synthesis, spectra and redox properties of mononuclear five-co-ordinate copper(II) complexes with non-communicable pyrazole/pyridyl containing ligands X-ray structure of [2,6-bis(3,5-dimethyl-pyrazol-1-ylmethyl)pyridine][2- (3,5-dimethylpyrazol-1-ylmethyl)pyridine]-copper(II) diperchlorate. *Polyhedron* 1999, 18, 1743—1750.
- (55) Gupta, R.; Mukherjee, R. Synthesis and properties of $[CuLCl_2]$ and $[CuL(N_3)(OClO_3)] \cdot H_2O$ ($L = \alpha\alpha,\alpha\alpha'$ -bis(pyrazolyl)-*m*-xylene): X-ray structure of $[CuLCl_2]_2$. Polyhedron **2000**, 19, 719–724.
- (56) Singh, J.; Hundal, G.; Corbella, M.; Gupta, R. Synthesis, characterization and structures of copper(II) complexes with amide-based ligands: Unusual formation of a linear trimer and a zig-zag chain and their contrast magnetic behavior. *Polyhedron* **2007**, *26*, 3893–3903.
- (57) Xu, X. W.; Li, X. J.; Zhan, S. H.; Li, Y. T.; Wu, Z. Y.; Yan, C. W. Synthesis and structure of a new tetracopper(II) complex bridged both by oxamido and phenolato groups: Cytotoxic activity, and reactivity towards DNA and BSA. *J. Mol. Struct.* **2013**, *1039*, 28–36.
- (58) Gokhale, N. H.; Padhye, S. B.; Billington, D. C.; Rathbone, D. L.; Croft, S. L.; Kendrick, H. D.; Anson, C. E.; Powell, A. K. Synthesis and characterization of copper(II) complexes of pyridine-2-carboxamidrazones as potent antimalarial agents. *Inorg. Chim. Acta* **2003**, 349, 23–29.
- (59) Gupta, R.; Lal, T. K.; Mukherjee, R. Synthesis and properties of $[Cu(L^5)_2][ClO_4]_2$, H_2O having square planar and pseudo-octahedral

- geometries in the same unit cell, and anion-bound complexes $[Cu(L^5)_2X][ClO_4]$ (X = Cl⁻, NCS⁻, N₃⁻) [L⁵ = 2-(3,5-dimethylpyrazol-1-ylmethyl)pyridine]. *Polyhedron* **2002**, *21*, 1245–1253.
- (60) Bansal, D.; Gupta, R. Hydroxide-bridged dicopper complexes: Influence of secondary coordination sphere on structure and catecholase activity. *Dalton Trans.* **2017**, *46*, 4617–4627.
- (61) Matovic, Z. D.; Ristic, B.; Joksovic, M.; Trifunovic, S. R.; Pelosi, G.; Ianelli, S.; Ponticelli, G. Square-planar copper(II) complexes with a novel tetradentate amido-carboxylate ligand. Crystal structure of $[Co(H_2O)_6][Cu(mda)] \cdot 2H_2O$. Transition Met. Chem. **2000**, 25, 720–726.
- (62) Zhang, J.; Frankevich, V.; Knochenmuss, R.; Friess, S. D.; Zenobi, R. Reduction of Cu(II) in Matrix-Assisted Laser Desorption/Ionization Mass spectrometry. J. Am. Soc. Mass Spectrom. 2003, 14, 42–50
- (63) Bhaskar, G.; Prabhakar, S.; Prasada Raju, N.; Ramanjaneyulu, G. S. R Matrix-assisted Laser Desorption/ionization Studies on Transition Metal Complexes of Benzimidazole Thiosemicarbazones. *Eur. J. Mass Spectrom.* **2007**, *13*, 135–145.
- (64) Rosa, V.; Santos, C. I. M.; Welter, R.; Aullon, G.; Lodeiro, C.; Aviles, T. Comparison of the Structure and Stability of New $\alpha\alpha$ -Diimine Complexes of Copper(I) and Silver(I): Density Functional Theory versus Experimental. *Inorg. Chem.* **2010**, *49*, 8699–8708.
- (65) Ahmed, A.; Robertson, C. M.; Steiner, A.; Whittles, T.; Ho, A.; Dhanak, V.; Zhang, H. Cu(I)Cu(II)BTC A Microporous Mixed-valence MOF via Reduction of HKUST-1. RSC Adv. 2016, 6, 8902–8905.
- (66) Moulder, J. F.; Stickle, W. F.; Sobol, W. T.; Bomben, K. D. Handbook of X-ray Photoelectron Spectroscopy; Physical Electronics: 1992.
- (67) Deroubaix, G.; Marcus, P. X-ray Photoelectron Spectroscopy Analysis of Copper and Zinc Oxides and Sulphides. *Surf. Interface Anal.* **1992**, *18*, 39–46.
- (68) Kurmaev, E. Z.; Galakhov, V. R.; Fedorenko, V. V.; Elokhina, L. V. X-ray Emission, Photoelectron Spectra, and Electronic Structure of $Sr_2CuO_2F\delta_{2+\delta}$. Phys. Rev. B: Condens. Matter Mater. Phys. **1995**, 52, 2390–2394.
- (69) Rojas, M. L.; Fierro, J. L. G.; Tejuca, L. G.; Bell, A. T. Preparation and Characterization of LaMn x_{1-x} Cu $_x$ O $\lambda_{3+\lambda}$ Perovskite Oxides. *J. Catal.* **1990**, 124, 41–51.
- (70) Otamiri, J. C.; Anderson, S. L. T.; Anderson, A. Ammoxidation of Toluene by YBa₂Cu₃O_{6+x} and Copper Oxides: Activity and XPS Studies. *Appl. Catal.* **1990**, *65*, 159–174.
- (71) Nefedov, V. I.; Firsov, M. N.; Shaplygin, I. S. Electronic Structures of MRhO₂, MRh₂O₄, RhMO₄ and Rh₂MO₆ on the Basis of X-ray Spectroscopy and ESCA Data. *J. Electron Spectrosc. Relat. Phenom.* **1982**, 26, 65–78.
- (72) Uraev, A. I.; Vasilchenko, I. S.; Ikorskii, V. N.; Shestakova, T. A.; Burlov, A. S.; Lyssenko, K. A.; Vlasenko, V. G.; Kuz'menko, T. A.; Divaeva, L. N.; Pirog, I. V.; Borodkin, G. S.; Uflyand, I. E.; Antipin, M. Y.; Ovcharenko, V. I.; Garnovskii, A. D.; Minkin, V. I. Copper(II) Dimers with Ferromagnetic Intra- and Intermolecular Exchange Interactions Mendeleev. *Mendeleev Commun.* 2005, 15, 133–135.
- (73) Jotham, R. W.; Kettle, S. F. A. Spin-Exchange in Polynuclear Systems. *Inorg. Chim. Acta* **1970**, *4*, 145–149.
- (74) Boča, R.; Herchel, R. Antisymmetric Exchange in Polynuclear Metal Complexes. *Coord. Chem. Rev.* **2010**, 254, 2973–3025.
- (75) Calancea, S.; Reis, S. G.; Guedes, G. P.; Allão Cassaro, R. A.; Semaan, F.; López-Ortiz, F.; Vaz, M. G. F. A New Family of Multinuclear Mixed-ligand Copper(II) Clusters: Crystal Structures, Magnetic Properties and Catecholase-like Activity. *Inorg. Chim. Acta* 2016, 453, 104–114.
- (76) Ferrer, S.; Lloret, F.; Pardo, E.; Clemente-Juan, J. M.; Liu-Gonzalez, M.; Garcia-Granda, S. Antisymmetric Exchange in Triangular Tricopper(II) Complexes: Correlation among Structural, Magnetic, and Electron Paramagnetic Resonance Parameters. *Inorg. Chem.* **2012**, *51*, 985–1001.